COMMUN. MATH. SCI.
Vol. 15, No. 4, pp. 1041–1053

SCATTERING OF ELECTROMAGNETIC WAVES BY THIN HIGH CONTRAST DIELECTRICS II: ASYMPTOTICS OF THE ELECTRIC FIELD AND A METHOD FOR INVERSION*

DAVID M. AMBROSE†, JAY GOPALAKRISHNAN‡, SHARI MOSKOW§, AND SCOTT ROME¶

Abstract. We consider the full time-harmonic Maxwell equations in the presence of a thin, high-contrast dielectric object. As an extension of previous work by two of the authors, we continue to study limits of the electric field as the thickness of the scatterer goes to zero simultaneously as the contrast goes to infinity. We present both analytical and computational results, including simulations which demonstrate that the interior transverse component of the electric field has limit zero, and a rigorous asymptotic approximation accurate outside of the scatterer. Finally, we propose an inversion method to recover the geometry of the scatterer given its two-dimensional plane and we present numerical simulations using this method.

Keywords. scattering; Maxwell's equations; asymptotics; thin dielectric; inverse problem; perfectly matched layer.

AMS subject classifications. 78A45; 78A46; 45E99; 35C20.

1. Introduction

Motivated by the study of photonic band gap materials, we are interested in understanding precisely the behavior of the solutions to Maxwell's equations in the presence of a thin dielectric scatterer of finite extent which has a large index of refraction. In certain regimes, such as when the thickness of the slab is on the order of the reciprocal of the squared index of refraction, it is possible to use two-dimensional periodic structures which are known to have band gaps on a thin slab, and still observe band-gap-like effects [9]. Unfortunately, repeated numerical simulations for such problems are expensive since the geometry is truly three dimensional. Here, we follow an asymptotic approach introduced in [7] and continued in [2] and [1] with the goals of developing streamlined computational methods and gaining insight into material design.

In the paper [7], Santosa, Zhang, and the third author proposed an approximate method to compute scattered fields from thin high contrast dielectric structures for the reduced model of the Helmholtz equation. A perturbation approach based on expansions with respect to the thickness of the scatterer (or the reciprocal of the squared refractive index) was applied. This asymptotic approach was extended to Maxwell's equations in the presence of smoothly varying dielectrics in [2]. The advantage of these methods is that they reduce the complexity of the computation by one dimension (i.e., a

*Received: August 4, 2015; accepted (in revised form): November 28, 2016. Communicated by Guillaume Bal.
David M. Ambrose is grateful to the National Science Foundation for support through grant DMS-1515849. Jay Gopalakrishnan is grateful to the National Science Foundation for support through grant DMS-1318916. Scott Rome and Shari Moskow are grateful to the National Science Foundation for support through grants DMS-1108858 and DMS-1411721. The authors would like to thank Kimberly Kilgore for allowing us to use her code to solve the system of three dimensional integral equations.

†Department of Mathematics, Drexel University, 3141 Chestnut St., Philadelphia, PA 19104; (dma68@drexel.edu).
‡Portland State University, PO Box 751, Portland, OR 97207-0751; (gjay@pdx.edu).
§Department of Mathematics, Drexel University, 3141 Chestnut St., Philadelphia, PA 19104; (moskow@math.drexel.edu).
¶Department of Mathematics, Drexel University, 3141 Chestnut St., Philadelphia, PA 19104; (romescott@gmail.com).

three-dimensional volume integral equation reduces to a set of two-dimensional integral equations). This leads to a highly efficient computational method for obtaining the scattered field anywhere in $\mathbb{R}^3$: one can first inexpensively solve for the field using the dimensionally reduced system inside the scatterer, and then use this approximation as input into an integral equation with the fundamental solution to obtain the total field outside the scatterer.

In the paper [1], the first and third authors studied the same scattering problem, using the full three-dimensional Maxwell time-harmonic system, allowing for jumps in the material with respect to a constant background. Here we will use a formulation developed there; this formulation is similar to the integral equation Theorem 9.1 of [4], but has an added surface term which takes the jumps into account. We found that surface terms arising from material jumps do indeed impact the resulting system and approximations. We showed under certain regularity conditions that the normal component of the electric field on the interior boundary of the scatterer converges to zero, and that the component of the electric field transverse to the plane of the scatterer converges to zero in the *interior* of the scatterer. Here we provide full three dimensional numerical experiments demonstrating that this convergence is indeed happening. We also use the formulation from [1] to derive the jump condition for the electric field across the boundary of the scatterer.

We also derive an asymptotic approximation valid outside the scatterer, which suggests an inversion method. The inversion method requires that the plane of the scatterer be known, and is qualitative in the sense that the geometry of the scatterer can be captured, but not the actual profile of the refractive index. This is a quite natural assumption for thin slab photonic band gap materials since in applications their planar orientation and position is known. If the application is such that the plane of the scatterer is unknown apriori, one could potentially first find it numerically by other means, but we do not explore that here. To produce synthetic data we use both a coarse discretization of the integral formulation from [1] and a completely unrelated finite element method for Maxwell in free space. We test our inversion method using a single incident wave and present our recovered images.

This paper is organized as follows. Section 2 contains our asymptotic results about the scattering problem. Specifically, we present the problem formulation and prior results in Section 2.1 and we examine the layer potential limits and the resulting jump conditions in Section 2.2. In Section 2.3 and we state our theorems about the limiting system and present numerical evidence that the transverse component of the field inside the scatterer is indeed vanishing. Section 2.4 contains our asymptotic result for the field outside the scatterer. Section 3 contains our proposed inversion method and the numerical results. This linear qualitative inversion method is based on the asymptotic formula derived in Section 2.4. We describe the method in Section 3.1 present numerical results in Section 3.2.

2. The high-contrast maxwell scattering problem

In this section we describe our results about the asymptotics of the electric field inside the scatterer, present numerical evidence supporting these results, and develop an asymptotic formula which is valid outside of the scatterer.

2.1. Formulation and prior results. Consider the time-harmonic Maxwell equation with a thin scatterer present,

$$\nabla \times \nabla \times E - k^2 n^2 E = 0 \quad \text{on } \mathbb{R}^3, \tag{2.1}$$

where E is the electric field, $k>0$ is the normalized temporal frequency, and n^2 denotes the squared index of refraction. (In our study, we assume that magnetic permeability, μ, is simply equal to 1.) We investigate the case where the scatterer is given by

$$\Omega_h = \Omega \times (-h/2, h/2)$$

with Ω a bounded open subset of $\mathbb{R}^2$. Let us assume that Ω has a smooth boundary curve, so that the boundary of the cylinder $\partial\Omega_h$ is Lipschitz. In the earlier work [2], which uses a formulation from [4], the authors examined solutions of (2.1) as $h \to 0$ under the assumption that n^2 is smooth. Here, as in [1], we instead assume that n^2 is given by

$$n^2(x,z) = \begin{cases} 1 & |z| > h/2, \\ \epsilon_0/h & |z| < h/2, x \in \Omega \\ 1 & |z| < h/2, x \notin \Omega, \end{cases} \tag{2.2}$$

$x \in \mathbb{R}^2$ and $z \in \mathbb{R}$, and we do not smooth out the jump. We assume that ϵ_0 is a constant and h is a dimensionless small parameter, which indicates the high contrast nature of the scatterer. Notice that Ω is not assumed to be convex, so any holes in Ω will be captured in $\partial\Omega_h$. We will use the notation $(E\cdot\nu)^-(x,z)$ to indicate the limit from the interior of $E\cdot\nu$ at (x,z), where $(x,z) \in (\partial\Omega \times (-h/2,h/2)) \cup (\Omega \times \{-h/2, h/2\})$, and where ν will always indicate the outward unit normal to this surface. Note that this is is the boundary $\partial\Omega_h$ without its corners, so that the normal is well defined. For our investigation we will use the integral formulation of (2.1) from [1]: Assume that $E \in H_{loc}(\mathrm{curl}, \mathbb{R}^3)$ is the unique radiating solution of (2.1). If additionally $E \in C^0(\overline{\Omega_h}) \cap H^1(\Omega_h)$, then E will solve the coupled system

$$\begin{aligned} E(x,z) = {} & E_{\mathbf{i}}(x,z) + k^2 \int_{\Omega_h} \phi(x,z,x',z')(n^2(x',z')-1)E(x',z')\,dx'\,dz' \\ & - \nabla_{x,z} \int_{\partial\Omega_h} \phi(x,z,x',z')(n^2(x',z')-1)(E\cdot\nu')^-(x',z')\,d\sigma', \end{aligned} \tag{2.3}$$

for any $(x,z) \in \mathbb{R}^3 \setminus \partial\Omega_h$, and

$$\begin{aligned} (E\cdot\nu)^-(x,z) = {} & E_{\mathbf{i}}(x,z)\cdot\nu + k^2\nu \cdot \int_{\Omega_h} \phi(x,z,x',z')(n^2(x',z')-1)E(x',z')\,dx'\,dz' \\ & - \int_{\partial\Omega_h} \partial_{\nu_x}\phi(x,z,x',z')(n^2(x',z')-1)(E\cdot\nu')^-(x',z')\,d\sigma' \\ & - \frac{1}{2}(n^2(x,z)-1)(E\cdot\nu)^-(x,z), \end{aligned} \tag{2.4}$$

for any $(x,z) \in \partial\Omega_h$. Here $d\sigma'$ indicates the surface measure with respect to the primed variables and ν' is the outward unit normal to $\partial\Omega_h$ at the point (x',z'). The incident wave $E^{\mathbf{i}}$ satisfies

$$\nabla \times \nabla \times E^{\mathbf{i}} - k^2 E^{\mathbf{i}} = 0, \tag{2.5}$$

and ϕ is the fundamental solution to the Helmholtz equation in $\mathbb{R}^3$,

$$\phi(x,z,x',z') = \frac{1}{4\pi} \frac{e^{ik|(x,z)-(x',z')|}}{|(x,z)-(x',z')|}. \tag{2.6}$$

In [1], it was proven that if $E_3 \in C^{0,\alpha}(\Omega_h)$ with a bound independent of h, then $E_3(x,0) \to 0$ as $h \to 0$. Furthermore, it was shown formally that the limiting system for E in the scatterer was as follows:

$$E_1^{(0)}(x) = (E_{\mathbf{i}})_1(x,0) + k^2 \int_\Omega \phi(x,0,x',0)\epsilon_0 E_1^{(0)}(x')dx', \tag{2.7}$$

$$E_2^{(0)}(x) = (E_{\mathbf{i}})_2(x,0) + k^2 \int_\Omega \phi(x,0,x',0)\epsilon_0 E_2^{(0)}(x')dx', \tag{2.8}$$

$$E_3^{(0)}(x) = 0. \tag{2.9}$$

for $x \in \Omega$. Sections 2.2 and 2.3 of the current manuscript will provide further evidence for the asymptotic formula (2.9).

REMARK 2.1. In the previous paper [1], Theorem 2.1 contains a sign error, and the affected formula (17) from [1] is corrected in (2.4) above. This correction does not change the results of [1], except that in Theorem 3.1 of [1], the formula for the limiting operator $\tilde{T}_0$ is incorrect. The correct operator is given by the matrix

$$\tilde{T}_0 = \begin{pmatrix} 0 & -1/2 & 0 \\ -1/2 & 0 & 0 \\ -1/4R & 1/4R & 0 \end{pmatrix}. \tag{2.10}$$

2.2. Layer potential limits. In this section, we will use *a priori* assumptions on the regularity of the solutions and on boundedness with respect to h to calculate the limit of $(E\cdot\nu)^-$. He we use layer potentials to show explicit results about the behavior of $(E\cdot\nu)^-$ as $h \to 0$, and obtain a formula for the jump across the top and bottom of the scatterer.

We will assume we have a solution E to the system of integral equations (2.3) and (2.4) on $\mathbb{R}^3$. We will continue to use the notation that $x, x' \in \mathbb{R}^2$, while $z, z' \in \mathbb{R}$. Note that in Equation (2.4), there is a normal derivative of the single layer potential acting on the interior normal boundary trace $(E\cdot\nu)^-$, so its regularity properties are those of a double layer potential. Since our scatterer is a cylinder, its boundary is merely Lipschitz, and the double layer potential needs to be defined by principal value on the corners. This is well known, however, and double layer potentials are well defined on Lipschitz domains [12, 6]. So we define

$$T_h^* : L^2(\partial\Omega_h) \to L^2(\partial\Omega_h)$$

to be given by

$$T_h^*(f)(x,z) = \int_{\partial\Omega_h} \partial_{\nu_{x,z}} \phi(x,z,x',z') f(x',z')\, d\sigma'. \tag{2.11}$$

where the principal value is implied when necessary. This operator is in fact the adjoint of the double layer potential operator. From Equation (2.4), the interior limit to the boundary satisfies

$$\begin{aligned}(E\cdot\nu)^-(x,z) = {} & E_{\mathbf{i}}(x,z)\cdot\nu(x,z) + k^2\nu(x,z)\cdot\int_{\Omega_h} \phi(x,z,x',z')(n^2(x',z')-1)E(x',z')\,dx'\,dz' \\ & - \left(\frac{1}{2}I + T_h^*\right)((n^2-1)^-(E\cdot\nu)^-)(x,z)\end{aligned} \tag{2.12}$$

almost everywhere (recall that ν is the unit outward normal). For clarity, our convention will be to write

$$(n^2-1)(E\cdot\nu)^-(x,z) := (n^2(x,z)-1)^-(E(x,z)\cdot\nu(x,z))^-.$$

We rewrite (2.12) as

$$\left(\frac{1}{2}I+T_h^*\right)((n^2-1)(E\cdot\nu)^-)(x,z) = -(E\cdot\nu)^-(x,z)+E_{\mathbf{i}}(x,z)\cdot\nu(x,z) + k^2\nu(x,z)\cdot\int_{\Omega_h}\phi(x,z,x',z')(n^2(x',z')-1)E(x',z')\,dx'\,dz'. \quad (2.13)$$

Fix $(x,z)\in\partial\Omega_h$ such that (x,z) is not on the corners, i.e., $(x,z)\notin\partial\Omega\times\{-h/2,h/2\}$. For technical reasons we must exclude the (x,z) on the corners, and for convenience, we will not always mention that such points are excluded in what follows. We will now derive a jump condition for $E\cdot\nu$ across the scatterer. Note that the Equation (2.3) for the electric field holds on the exterior of Ω_h. In particular for $(\hat{x},\hat{z})\in\mathbb{R}^3\setminus\overline{\Omega_h}$, we have that the following holds:

$$E(\hat{x},\hat{z}) = E^{\mathbf{i}}(\hat{x},\hat{z}) + k^2\int_{\Omega_h}\phi(\hat{x},\hat{z},x',z')(n^2(x',z')-1)^-E(x',z')\,dx'\,dz' - \nabla_{\hat{x},\hat{z}}\int_{\partial\Omega_h}\phi(\hat{x},\hat{z},x',z')(n^2(x',z')-1)(E\cdot\nu')^-(x',z')\,d\sigma'. \quad (2.14)$$

By taking the inner product with the unit outward normal and limiting to (x,z) from the exterior in (2.14), the last term on the right-hand side becomes the normal derivative of a single layer potential with density $(1-n^2)(E\cdot\nu)^-$. We then take the limit with an argument as in Chapter 3 in [5],

$$\lim_{\substack{(\hat{x},\hat{z})\to(x,z)\\(\hat{x},\hat{z})\in\mathbb{R}^3\setminus\Omega_h}}\nu_{(\hat{x},\hat{z})}\cdot\nabla_{\hat{x},\hat{z}}\int_{\partial\Omega_h}\phi(\hat{x},\hat{z},x',z')(n^2(x',z')-1)(E\cdot\nu')^-(x',z')\,d\sigma' = \left(-\frac{1}{2}I+T_h^*\right)((n^2-1)(E\cdot\nu)^-)(x,z), \quad (2.15)$$

and therefore by isolating this term on the left hand side we have

$$-\left(-\frac{1}{2}I+T_h^*\right)((n^2-1)(E\cdot\nu)^-)(x,z) = (E\cdot\nu)^+(x,z)-(E_{\mathbf{i}}\cdot\nu)(x,z)-k^2\nu_{(x,z)}\cdot\int_{\Omega_h}\phi(x,z,x',z')(n^2(x',z')-1)E(x',z')\,dx'\,dz'. \quad (2.16)$$

Adding (2.13) to (2.16) yields the equation for the density:

$$(n^2(x,z)-1)(E\cdot\nu)^-(x,z) = (E\cdot\nu)^+(x,z)-(E\cdot\nu)^-(x,z) \quad (2.17)$$

almost everywhere on $\partial\Omega_h$.

For the following theorem we need to make the assumption that the exterior normal component of the field is bounded uniformly in h. Note that this was true for the Helmholtz case [7], and we expect that it is true for Maxwell. Numerical results in the

next subsection are consistent with this; however, a rigorous result is not known to the authors.

THEOREM 2.1. *Let n^2 be given by (2.2). Assume $E \in C^0(\overline{\Omega_h}) \cap H^1(\Omega_h)$ solves the coupled system defined by (2.3) and (2.4), and assume that $(E\cdot\nu)^+$ is bounded uniformly in h on $\partial\Omega_h$. Then,*

$$\|(E\cdot\nu)^-\|_{L^\infty(\partial\Omega_h)} = O(h) \tag{2.18}$$

Proof. From (2.17),

$$\frac{\epsilon_0}{h}(E\cdot\nu)^-(x,z) = (E\cdot\nu)^+(x,z). \tag{2.19}$$

Since $(E\cdot\nu)^+$ is bounded uniformly in h, the result follows from (2.19). ∎

2.3. Asymptotics of the electric field inside the scatterer. In the prior work [1], the authors proved the following theorem:

THEOREM 2.2. *Let $E_3 \in C^\alpha(\Omega_h)$ for some $0<\alpha\le 1$ solve the coupled system (2.3), (2.4), and assume that*

$$\|E_3\|_{C^\alpha(\Omega_h)} \le M_\alpha$$

where M_α is independent of h. Then, pointwise for $x\in\Omega_h$, there exists C depending on α and possibly x such that, for $\alpha<1$, we have

$$|E_3(x)| \le C M_\alpha h^\alpha,$$

and for $\alpha = 1$ we have

$$|E_3(x)| \le C M_1 h|\log h|$$

where C is independent of h.

As the statement of Theorem 2.2 indicates, we are able, under some assumptions about the behavior of the electric field as h vanishes, to conclude that E_3 vanishes pointwise. One may quite reasonably ask, then, whether either these hypotheses or this conclusion do in fact hold. While we do not have an analytical answer at present for this interesting question, we present two facts supporting the affirmative.

The first is a theorem that shows that the conclusion that E_3 vanishes also follows from alternate hypotheses; namely, the following theorem has been proved in [10]:

THEOREM 2.3. *Let $E \in C^0(\overline{\Omega_h}) \cap H^1(\Omega_h)$ solve the coupled system defined by (2.3) and (2.4), and assume that E_3 is uniformly bounded in h for $(x,z)\in\Omega_h$. If $(E\cdot\nu)^+$ is equicontinuous with respect to h, and both $\|(E\cdot\nu)^+\|_{L^\infty(\partial\Omega_h)}$ and $\|E_3\|_{L^\infty(\Omega_h)}$ are bounded uniformly in h, then for $(x,\zeta)\in\Omega\times(-1/2,1/2)$,*

$$\lim_{h\to 0} E_3(x,h\zeta) = 0.$$

The second is in the form of numerical evidence that supports the conclusion that E_3 does indeed vanish inside the scatterer as h vanishes. For these simulations, we consider a thin cylindrical dielectric of radius 0.25 and thickness h set at the origin in

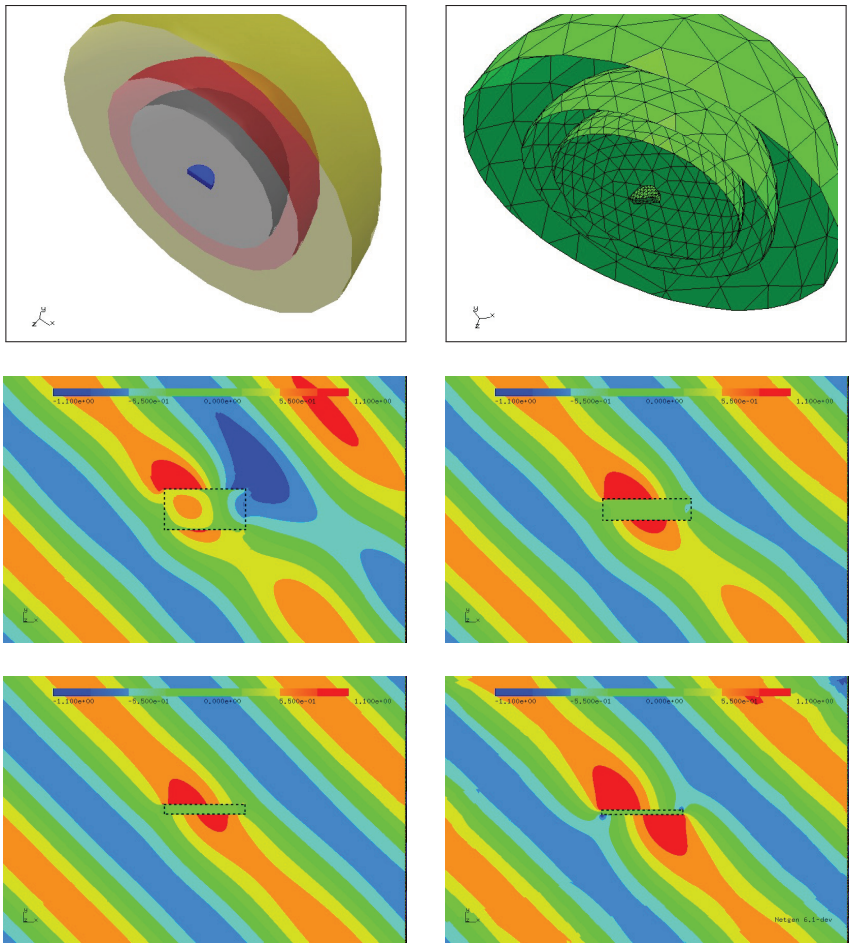

FIG. 2.1. Top left: *Half of the simulation geometry consists of a cylindrical dielectric of radius* 1/4*, enclosed within a spherical PML in the region between the concentric spheres of radii* 2 *and* 3. Top right: *Edges of a tetrahedral mesh of the simulation domain that lie on the same surfaces shown top left.* The remainder *of the figures show the real part of the transverse (y) component of the total field for* $h = 1/4, 1/8, 1/16$, *and* $1/32$ *along the* $z = 0$ *cross section shown in the top row. The dielectric boundary is shown by dotted lines.*

the xz plane. The squared index of refraction n^2 is given by (2.2) with $\epsilon_0 = 1$. The scattered wave $E^{\mathbf{s}} = E - E^{\mathbf{i}}$ satisfies

$$\nabla \times \nabla \times E^{\mathbf{s}} - k^2 n^2 E^{\mathbf{s}} = k^2 (n^2 - 1) E^{\mathbf{i}}$$

in $\mathbb{R}^3$ together with the standard outgoing radiation boundary conditions at infinity. In order to compute an approximation to the outgoing $E^{\mathbf{s}}$, we enclose the dielectric inside a spherical perfectly matched layer (PML) [3] beginning at radius 2 (see Figure 2.1). Then we truncate the infinite domain at radius 3. The solution, while unaltered before the onset of PML, exponentially decays (without any spurious reflections) within the PML region. Hence at the outer radius we may impose the perfect electric boundary condition. The truncated domain is then meshed by a tetrahedral mesh for moderate values of $h \geq 1/16$. For smaller values of h, tetrahedral meshing leads to a very large

number of elements, so a combination of prismatic elements within the dielectric and tetrahedral elements outside was used. The equation was then discretized using Nedelec elements [8] of degree 3. An incident wave impinging on the dielectric at 45 degree angle gave the source term for a finite element approximation of the scattered and total wave. The entire simulation was implemented within the NGSolve [11] package and approximations to the scattered field were computed for various values of h. Note that the computational geometry is such that y (not z, as before) is the transverse direction, so let us temporarily use E_y to denote the transverse field.

The computed approximations of E_y are shown in Figure 2.1. Its values inside and outside the dielectric are interesting. First, the values of E_y outside the dielectric appear to remain bounded for $h = 1/4, \ldots, 1/32$. Although these results are only for one incidence angle, our numerical experience suggests that the equicontinuity assumption on $(E \cdot \nu)^+$ may very well hold. More important for the present purpose is the values of E_y inside the dielectric. The plots show that values of E_y are smaller inside the dielectric and appear to become smaller as h is decreased. More quantitative information was extracted from the simulation in the form of approximation to $\|E_y\|_{L^2(\Omega_h)}$ for each value of h, denoted by $\|E_y\|_{2,h}$ and displayed in Figure 2.2. An approximation that scales like the $L^\infty(\Omega_h)$-norm is denoted by $\|E_y\|_{\infty,h} = \|E_y\|_{2,h}/\sqrt{h}$ and is shown in the same figure. (Here, we divide the L^2 norm by $\sqrt{h}$ to adjust for the fact that the volume is going to zero like h.) Slopes of the regression lines approximating the convergence curves are also marked in the figure. We see that in the reported h-range, $\|E_y\|_{\infty,h}$ appears to go to zero faster than $O(h)$.

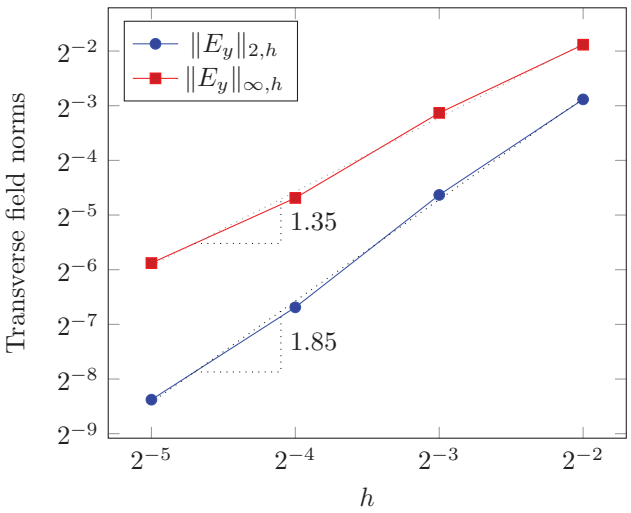

FIG. 2.2. *Norms of transversal electric field for various values of dielectric thickness h*

2.4. Asymptotics outside the scatterer. We gave numerical evidence above that the transverse component of the total field, E_3, becomes small *inside* the scatterer. Here we prove a result about its behavior outside the scatterer which is potentially useful for inversion.

THEOREM 2.4. *Let $E \in C^0(\overline{\Omega_h}) \cap H^1(\Omega_h) \cap H_{loc}(curl, \mathbb{R}^3)$ solve the coupled system defined by (2.3) and (2.4) on all of $\mathbb{R}^3$. Assume $(E \cdot \nu)^+$ is equicontinuous with respect*

to h, and both $\|(E\cdot\nu)^+\|_{L^\infty(\partial\Omega_h)}$ and $\|E_3\|_{L^\infty(\Omega_h)}$ are bounded uniformly in h. Then for $(x,z)\in\mathbb{R}^3\setminus\overline{\Omega_h}$,

$$E_3(x,z)=E_{\mathbf{i},3}(x,z)-\int_{\Omega\times\{-h/2,h/2\}}\frac{\partial}{\partial z}\phi(x,z,x',0)(n^2(x',z')-1)(E\cdot\nu)^-(x',z')\,dx'+o(1).$$

Proof. We will use the Equation (2.3) for (x,z) outside of the scatterer:

$$\begin{aligned}E_3(x,z)=&E_{\mathbf{i},3}(x,z)+k^2\int_{\Omega_h}\phi(x,z,x',z')(n^2(x',z')-1)E_3(x',z')\,dx'\,dz'\\&-\int_{\partial\Omega_h}\frac{\partial}{\partial z}(x,z,x',z')(n^2(x',z')-1)(E(x',z')\cdot\nu)^-\,d\sigma'.\end{aligned}$$

In this case, none of the integrands are singular as $h\to 0$ (as they are when $x\in\Omega_h$). Thus we may use the fact that $|\Omega_h|=O(h)$, Theorem 2.3, the assumed bound on E_3 and dominated convergence to yield that the second term on the right hand side goes to 0. For the third term, Theorem 2.1 implies that the integral over the lateral side, $\partial\Omega\times(-h/2,h/2)$, goes to zero because the surface area of the domain, which is proportional to h, cancels with the h in the denominator of n^2 (see (2.2)).

Now, the remaining part of the third term is the integral on the top and bottom of the scatter, corresponding to $z'=\pm h/2$. In both cases we will replace the kernel with its value at $z'=0$. Using Theorem 2.1, the remainder can be bounded as follows:

$$\begin{aligned}&\left|\int_{\Omega\times\{-h/2,h/2\}}\left(\frac{\partial}{\partial z}\phi(x,z,x',z')-\frac{\partial}{\partial z}\phi(x,z,x',0)\right)(n^2(x',z')-1)(E\cdot\nu)^-(x',z')\,dx'\right|\\&\le C(\epsilon_0-h)\int_{\Omega\times\{-h/2,h/2\}}\left|\frac{\partial}{\partial z}\phi(x,z,x',z')-\frac{\partial}{\partial z}\phi(x,z,x',0)\right|dx'.\end{aligned}\tag{2.20}$$

Since (x,z) is external to the scatterer, the integrand on the right-hand side of (2.20) is smooth. Since $z'\in\{-h/2,h/2\}$, we see that the right-hand side of (2.20) limits pointwise almost everywhere to zero. This implies the result. ∎

3. A qualitative inversion method

In this section we describe and test numerically our method for inversion.

3.1. Outline of method. Here we propose a method which, under the assumption that one knows the plane of the scatterer slice $\Omega\times\{0\}$, can recover the location of Ω within this plane. One feature of the proposed approach is that it uses a two-dimensional integral to recover the position of the object. In this sense, it reduces the complexity of the calculation by one dimension at the cost of having to know *a priori* the plane of the scatterer.

The above Theorem 2.4 says that asymptotically, the transverse component of the scattered field is close to an integral operator acting on a function with support on the scatterer. So assuming the hypotheses of Theorem 2.4 are met, for $(x,z)\in\mathbb{R}^3\setminus\Omega_h$,

$$E_3(x,z)-E_{\mathbf{i},3}(x,z)=\int_{\mathbb{R}^2}\frac{\partial}{\partial z}\phi(x,z,x',0)g(x')\,dx'+o(1),\tag{3.1}$$

as $h\to 0$. We may attempt, then, to invert the integral operator to find the unknown g,

$$g(x')=:-\mathbb{1}_\Omega(x')\hat{g}(x')\tag{3.2}$$

whose support is on Ω. Such an inversion would potentially recover the location and shape of Ω. Note that we have implicitly assumed that we know the thin scatterer lies centered on the $z=0$ plane. Also, the unknown g should be the limit of the sum of $(n^2-1)(E\cdot\nu)^-$ on the top and bottom, and hence it depends on the incident wave.

In the experiments that follow, we use only a single incident wave $E^{\mathbf{i}}$ so that g is fixed, and read the data $\Phi = E_3 - (E^{\mathbf{i}})_3$ at a set of receiver points. Based on the above, we assume that

$$\Phi(x,z) \approx \int_{\mathbb{R}^2} \frac{\partial}{\partial z}\phi(x,z,x',0)g(x')\,dx', \tag{3.3}$$

that is, we ignore the $o(1)$ term from (3.1). We then discretize and invert using a pseudoinverse obtained by truncating singular values to image the support of g.

3.2. Numerical results. For our experiments, we will try to image the support of a scatterer with refractive index in the form (2.2). That is, our scatterer will be a cylindrical object of the form $\Omega\times[-h/2,h/2]$ where Ω sits on the $z=0$ plane. For the trials, we generate synthetic data by either the completely independent finite element solver for the PDE (2.1) described in Section 2.3, or by solving the 3-d integral equation formulation (2.3), (2.4). We use only a single incident plane wave

$$E_{\mathbf{i}}(x,z) = pe^{i\eta\cdot(x,z)}$$

where η is of the form $(|\xi|\cos\theta,|\xi|\sin\theta,\sqrt{k^2-|\xi|^2})$ and $p\cdot\eta=0$. In all cases we chose $\epsilon_0=1.1$ and $k=1$. The figures in this section show the absolute value of the recovered g from (3.2). We will vary our values of h, and note that from Theorem 2.4, one would expect the image to become more accurate as h decreases.

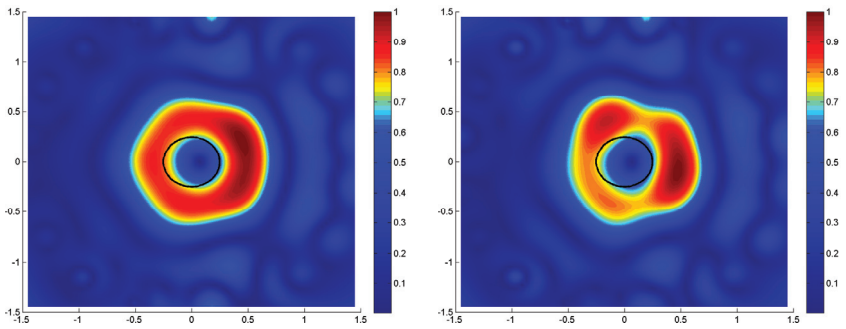

FIG. 3.1. *Image of recovered Ω (magnitude of g) for $h=1/8$, left, $h=1/64$, right. Initial wave parameters: $\theta=0$, $\xi=0$, $p=(-(\sqrt{2}/2)i,\sqrt{2}/2,0)^T$. Here Ω is a ball of radius $1/4$ centered at the origin.*

In our first example, Ω is a disk of radius $1/4$ centered at the origin and $\epsilon_0=1$. We used the finite element solver for full three dimensional Maxwell described in Section 2.3 to generate synthetic data, with 154 receiver points around a sphere of radius 2 centered at the origin, equally spaced in the spherical angular coordinates (θ,ϕ). The object is assumed to be known to be within this sphere. One can see in Figure 3.1, where we graph $|g(x,y)$, that the general location of the scatterer is found, despite the fact that $h=1/8$ is not very small. However, the size of the scatterer is significantly overestimated. For smaller $h=1/64$, the inversion method performed approximately just as well, but not significantly better. Figure 3.2 shows the behavior of the singular values.

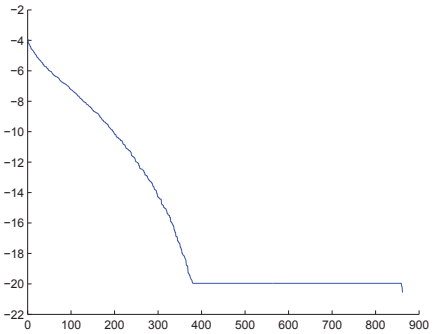

FIG. 3.2. *A graph of the singular values of the system from Figure 3.1 showing its ill-posedness. The y-axis is* $\log_{10}$ *scale.*

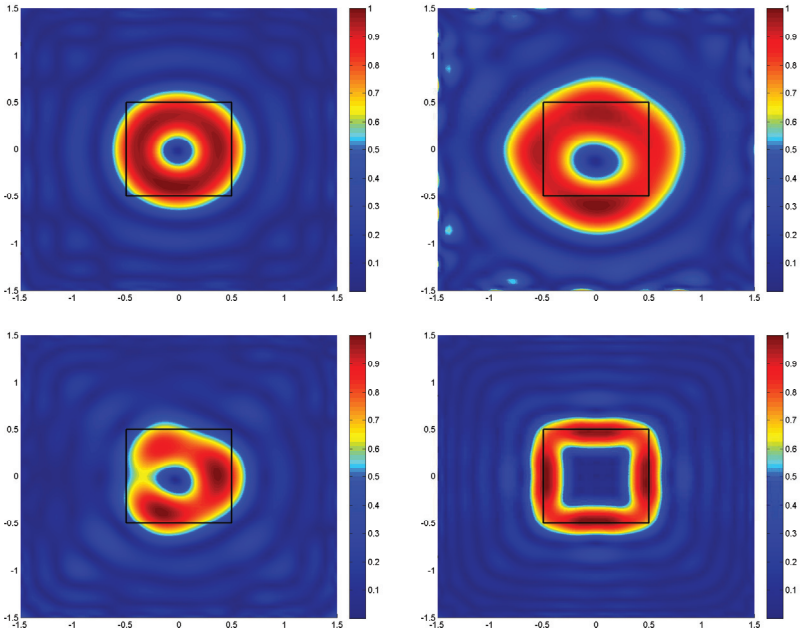

FIG. 3.3. *Generated images of the scatterer (magnitude of g) for* $h=1$ *and* .1 *on the top row and* $h=.01$ *and* .001 *on the bottom row respectively. Number of singular values used for inversion varied for each image to optimize resulting image.*

In our second example, Ω is a square of length $1/2$, and we will try to image the object for various values of h. Here our simulated data is generated by the integral equation system (2.3) and (2.4). Using the finite element method for the PDE (2.1) is clearly preferable from an "inverse crime" point of view, since the methods are totally unrelated. However, by using a somewhat coarse grid for our forward solver, we were able to obtain data for much smaller values of h by solving the integral equations. In this example 862 receivers were used, and the initial wave was given by $p=(-i/\sqrt{2},1/\sqrt{2},0)$ and $\eta=(0,0,1)$. Figure 3.2 shows a graph of the singular values for the system we inverted to generate Figure 3.3, which is of course the same as in the previous example.

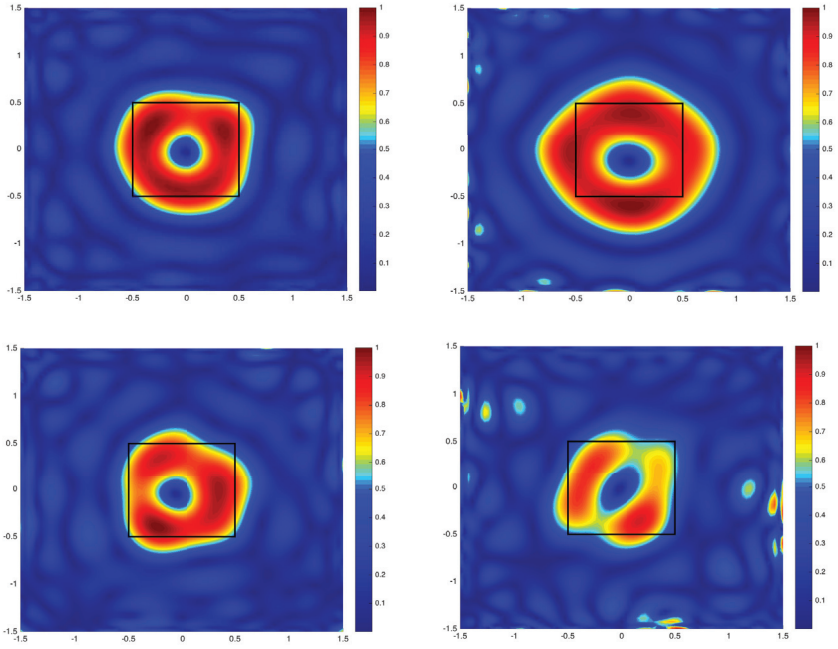

FIG. 3.4. *Generated images of the scatterer (magnitude of g) with* 1% *scaled noise added to data. Here* $h=1$ *(top left)* $h=.1$ *(top right),* $h=.01$ *(bottom left) and* $h=.001$ *(bottom right). More regularization was needed with the addition of noise.*

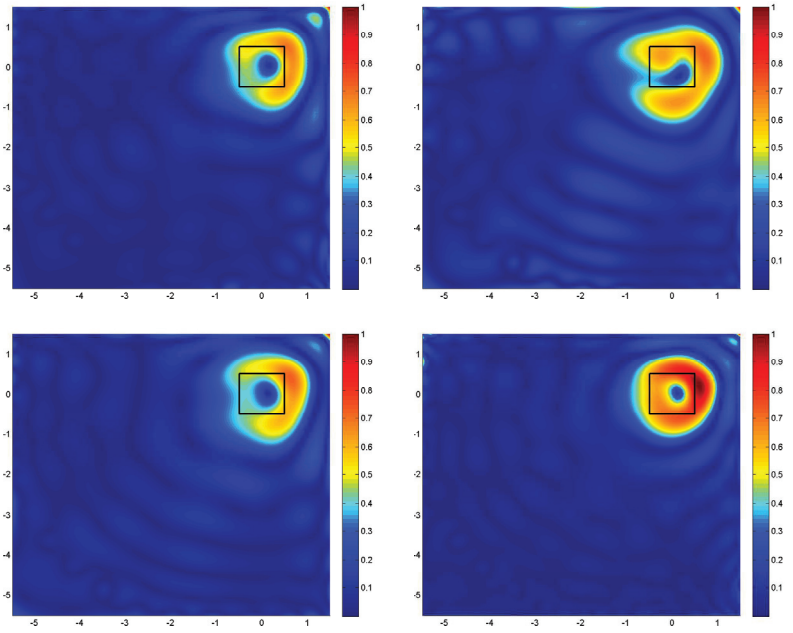

FIG. 3.5. *Generated images of the scatterer (magnitude of g) in a larger search region for* $h=1$ *(top left),* $h=.1$ *(top right),* $h=.01$ *(bottom left) and* $h=.001$ *(bottom right).*

Although the integral equation system (2.3), (2.4) used to generate the data is different from the approximation (3.3) used for the inversion, since the approach is similar and our forward solver grid was coarse, this does invite concerns about the possibility of an "inverse crime". We therefore add a small amount of noise (1%) to the data from the above experiment and present the resulting images in Figure 3.4. Note that the images for small h are less sharp than before. This is due to having to regularize more in the presence of noise. However, the location region of the scatterer is found reasonably well.

The last experiment is the same as the previous one without noise, except that now the 862 receivers will be located on a sphere of radius 6. The scatterer still occupies $[-.5,.5]^2$, so it is appearing towards the corner of the search region. Note the inversion procedure is finding the location correctly.

One observation from all of the figures is that the unknown g appears to be small in the interior of the scatterer in addition to the exterior, resulting in images which pick up a region around the boundary of the planar object. This is not unlike the single scattering captured by the Born approximation, another linearization which is valid for low contrast media as opposed to the high contrast refractive index assumed in the model here.

In summary, the proposed inversion method could potentially be useful for determining the location and shape of a scatterer of the form (2.2), if the plane of the scatterer is known, and particularly for small h. An advantage of the proposed method in this case is the fact that the computations become two dimensional. Furthermore, only one incident wave was used, and the images could potentially be improved by optimizing over a larger number of incident waves.

REFERENCES

[1] D.M. Ambrose and S. Moskow, *Scattering of electromagnetic waves by thin high contrast dielectrics: effects of the object boundary*, Commun. Math. Sci., 11:293–314, 2013.

[2] H. Ammari, H. Kang, and F. Santosa, *Scattering of electromagnetic waves by thin dielectric planar structures*, SIAM J. Math. Anal., 38:1329–1342, 2006.

[3] J.-P. Berenger, *A perfectly matched layer for the absorption of electromagnetic waves*, J. Comput. Phys., 114:185–200, 1994.

[4] D. Colton and R. Kress, *Inverse Acoustic and Electromagnetic Scattering Theory*, Appl. Math. Sci., Springer, 93, 2013.

[5] D. Colton and R. Kress, *Integral Equation Methods in Scattering Theory*, Classics in Applied Mathematics, Society for Industrial and Applied Mathematics, 2013.

[6] M. Costabel, *Boundary integral operators on Lipschitz domains: elementary results*, SIAM J. Math. Anal., 19:613–626, 1988.

[7] S. Moskow, F. Santosa, and J. Zhang, *An approximate method for scattering by thin structures*, SIAM J. Appl. Math., 66:187–205, (electronic) 2005.

[8] J.-C. Nédélec, *A new family of mixed finite elements in* $\mathbf{R}^3$, Numer. Math., 50:57–81, 1986.

[9] O. Painter, R.K. Lee, A. Scherer, A. Yariv, J. O'Brien, P.D. Dapkus, and I. Kim, *Two-dimensional photonic band-gap defect mode laser*, Science, 284:1819–1821, 1999.

[10] S. Rome, *Asymptotic Methods in Inverse Scattering*, Doctoral dissertation, Drexel University, 2015.

[11] Schöberl, http://sourceforge.net/projects/ngsolve/.

[12] G. Verchota, *Layer potentials and regularity for the Dirichlet problem for Laplace's equation in Lipschitz domains*, J. Funct. Anal., 59:572–611, 1984.